Myosin II isoforms promote internalization of spatially distinct clathrin-independent endocytosis cargoes through modulation of cortical tension downstream of ROCK2

Jessica Wayt[a], Alexander Cartagena-Rivera[b], Dipannita Dutta[c], Julie G. Donaldson[a], and Clare M. Waterman[a,*]

[a]Cell and Developmental Biology Center, National Heart, Lung, and Blood Institute, [b]Section on Mechanobiology, National Institute of Biomedical Imaging and Bioengineering, National Institutes of Health, Bethesda MD 20814; [c]National Center for Advancing Translational Sciences, Department of Health and Human Services, Rockville, MD 20850

ABSTRACT **Although the actomyosin cytoskeleton has been implicated in clathrin-mediated endocytosis, a clear requirement for actomyosin in clathrin-independent endocytosis (CIE) has not been demonstrated. We discovered that the Rho-associated kinase ROCK2 is required for CIE of MHCI and CD59 through promotion of myosin II activity. Myosin IIA promoted internalization of MHCI and myosin IIB drove CD59 uptake in both HeLa and polarized Caco2 intestinal epithelial cells. In Caco2 cells, myosin IIA localized to the basal cortex and apical brush border and mediated MHCI internalization from the basolateral domain, while myosin IIB localized at the basal cortex and apical cell–cell junctions and promoted CD59 uptake from the apical membrane. Atomic force microscopy demonstrated that myosin IIB mediated apical epithelial tension in Caco2 cells. Thus, specific cargoes are internalized by ROCK2-mediated activation of myosin II isoforms to mediate spatial regulation of CIE, possibly by modulation of local cortical tension.**

Monitoring Editor
Carole Parent
University of Michigan

Received: Jul 22, 2020
Revised: Oct 27, 2020
Accepted: Dec 8, 2020

This article was published online ahead of print in MBoC in Press (http://www.molbiolcell.org/cgi/doi/10.1091/mbc.E20-07-0480) on December 16, 2020.

The authors declare no competing financial interests.

Author contributions: J.W. contributed to conceptualization, performing experiments, data analysis, and writing and editing the manuscript; A.C.-R. contributed to performing experiments, data analysis, review, and editing of the manuscript; D.D. contributed to conceptualization, performing experiments, data analysis, review, and editing of the manuscript; J.D. and C.W. contributed to conceptualization, funding acquisition, resources, supervision, project administration, writing, and editing the manuscript.

*Address correspondence to: Clare M. Waterman (watermancm@nhlbi.nih.gov).

Abbreviations used: CIE, clathrin-independent endocytosis; CME, clathrin-mediated endocytosis; FBS, fetal bovine albumin; FM-AFM, acoustic noncontact frequency-modulation atomic force microscopy; GPI, glycosylphosphatidylinositol; MHCI, major histocompatibility complex class I; PBS, phosphate-buffered saline; pCFL, cofilin phosphorylation; pRLC, phosphorylated regulatory light chain; RLC, regulatory light chain; ROCK, Rho-associated kinase; RT, room temperature; TBS, Tris-buffer saline.

INTRODUCTION

Endocytosis is the process whereby cells internalize membrane, surface proteins, fluid, and nutrients and is critical to cell homeostasis and survival. Endocytosis occurs by two distinct mechanisms: clathrin-mediated endocytosis (CME) and clathrin-independent endocytosis (CIE) (Thottacherry *et al*., 2019). The well-studied process of CME is driven by the formation of clathrin-coated pits and an ensemble of adapter and signaling proteins and is important for the internalization of specific surface proteins such as engaged receptors (Traub and Bonifacino, 2013). In contrast, CIE mediates constitutive bulk trafficking of fluid, membrane, and associated proteins (Sandvig *et al*., 2018). Although the membrane trafficking itinerary of many classical CIE cargo proteins has been established (Maldonado-Báez *et al*., 2013) and several subtypes with distinct molecular requirements have been identified (Radhakrishna and Donaldson, 1997; Sabharanjak *et al*., 2002; Naslavsky *et al*., 2003; Chadda *et al*., 2007; Boucrot *et al*., 2015; Renard *et al*., 2015), mechanistic insight into CIE is still lacking.

Endocytosis is a physical process in which the surface tension of the plasma membrane must be overcome to form a microscale

invagination, followed by fission to release a vesicle into the cytoplasm (Boulant *et al.*, 2011; Day *et al.*, 2015; Bucher *et al.*, 2018). In CME, membrane deformation and fission is driven at least in part by BAR domain-containing proteins and dynamin GTPases (Damke *et al.*, 1994). Several lines of evidence also suggest that actomyosin cytoskeletal forces may contribute to CME (Renard *et al.*, 2018) and myosin II has also been implicated in clustering cargo or scaffolding actin at the plasma membrane in CME (Levayer *et al.*, 2011; Chandrasekar *et al.*, 2014). In contrast, for CIE, some pathways utilize BAR domain-containing proteins (Sathe *et al.*, 2018; Renard *et al.*, 2020) and/or dynamin (Henley *et al.*, 1998; Gold *et al.*, 1999; Boucrot *et al.*, 2015), but others do not (Kumari and Mayor, 2008; Johnson *et al.*, 2017). Furthermore, although actin regulatory proteins such as Cdc42, RhoA, and Rac1 have been implicated in CIE (Sabharanjak *et al.*, 2002; Soriano-Castell *et al.*, 2017a; Hak *et al.*, 2018) a clear requirement for actin or myosin motors in CIE has not been demonstrated.

We undertook a limited siRNA screen to identify candidate proteins required for internalization of two CIE cargo proteins, the glycosylphosphatidylinositol (GPI)-anchored protein CD59 and the transmembrane protein major histocompatibility complex class I (MHCI) in HeLa cells, and uncovered a potential role for the Rho-associated kinase (ROCK) proteins. ROCK proteins are major regulators of the actomyosin cytoskeleton, with downstream targets including myosin II, the actin severing protein cofilin, and membrane-associated actin binding proteins of the ezrin-radixin-moesin (ERM) and adducin families (Amano *et al.*, 2010). ROCK proteins promote myosin II activity by phosphorylation of myosin II regulatory light chain (RLC) (Amano *et al.*, 1996) and by phosphorylation and inactivation of myosin light chain phosphatase (Kimura *et al.*, 1996). In addition, phosphorylation of LIM kinase by ROCK proteins leads to the phosphorylation and deactivation of cofilin's actin severing activity (Maekawa *et al.*, 1999). In this way, ROCK promotes contractility by simultaneously promoting motor activity and actin stabilization, and as such, contributes to a wide array of contractile cell functions (Riento and Ridley, 2003). Although ROCK is also known to regulate cortical tension (Bhadriraju *et al.*, 2007; Rauskolb *et al.*, 2014), whether this contributes to a role in CIE through effects on plasma membrane tension has not been explored.

RESULTS AND DISCUSSION

ROCK2, but not ROCK1, is required for CIE

We sought to determine the role of ROCK proteins in CIE. HeLa cells, which express both ROCK1 and ROCK2 (Figure 1A), were subjected to siRNA-mediated depletion of either ROCK protein and assayed for internalization of antibodies bound to MHCI or CD59 as CIE cargoes. Western blot analysis showed that siRNA reduced ROCK1 and 2 levels to less than 10% of nontargeting control (Figure 1A). Analysis of CIE-mediated internalization of MHCI or CD59 showed that silencing ROCK2 significantly decreased internalization of both MHCI and CD59 (Figure 1B) (to 68% and 47% of nontargeting control, respectively), although the effect on CD59 was more pronounced. In contrast, silencing ROCK1 did not inhibit uptake and in fact stimulated internalization of both cargoes (Figure 1B). Expression of an siRNA-resistant, myc-tagged ROCK2 in ROCK2-silenced cells (Figure 1C) rescued MHCI internalization to control levels (Figure 1D), while uptake of CD59 was partially restored (Figure 1E). Changes to endocytic uptake were specific to CIE cargo proteins, as internalization of the CME cargo protein transferrin was unaffected by knockdown of either ROCK1 or 2 (Figure 1F). Acute inhibition of ROCK proteins with either the pan-ROCK inhibitor H-1152 (1.5 μM) or the ROCK2-specific KD025 (10 μM) decreased internalization of both MHCI and CD59 or CD59 internalization alone, respectively (Figure 1G), while neither treatment affected transferrin uptake (Figure 1H).

These results show that ROCK2, but not ROCK1, is required for CIE. Although ROCK1 and ROCK2 share 94% sequence identity in their kinase domains (Julian and Olson, 2014) and are treated as redundant, unique roles for these two kinases have been identified in the phosphorylation of RLC and cofilin (Shi *et al.*, 2013; Greathouse *et al.*, 2018). Furthermore, a recent report suggested that ROCK1 is essential for clathrin-independent internalization of β1-integrin (Soriano-Castell *et al.*, 2017b), although they did not exclude a contribution by ROCK2.

ROCK2 promotes CIE through regulation of myosin II contractility

We next sought to determine whether ROCK2 mediates its effect on CIE through regulation of myosin II or cofilin. Western blot analysis showed that ROCK2 silencing or pharmacological ROCK inhibition decreased the levels of phosphorylated RLC (pRLC) and cofilin phosphorylation (pCFL). In contrast, silencing ROCK1 had no significant effect on pCFL and mildly increased pRLC, which might explain the increase in cargo uptake caused by silencing ROCK1 (Figure 2, A and B). The decreases in pRLC and pCFL levels induced by ROCK2 knockdown were mirrored by a decrease in peripheral actin arcs and stress fibers seen by phalloidin staining (Figure 2C), while ROCK1 silencing slightly increased peripheral lamellipodia and actin arcs. Thus, ROCK2, and not ROCK1, regulates pRLC and pCFL and ultimately CIE in HeLa cells.

We next sought to determine if the ROCK2 effectors, myosin II and cofilin, were involved in CIE. Inhibiting myosin II ATPase with blebbistatin (50 μM) significantly reduced uptake of both MHCI and CD59 (Figure 2D) and disrupted actin arcs and stress fibers (Figure 2F), while internalization of transferrin was unaffected (Figure 2E). In contrast, silencing cofilin by siRNA (Figure 2G) in fact enhanced MHCI internalization (Supplemental Figure S1A, left), while CD59 and transferrin uptake were unaffected (Figure 2K, Supplemental Figure S1A, right). Furthermore, both MHCI and CD59 internalization were enhanced in cofilin-silenced cells even at short times of endocytosis (5 and 10 min, Figure 2I), suggesting that inhibition of recycling was not involved. Fixation and staining showed that cofilin silencing promoted dense peripheral actin where endosomes containing both cargo proteins were localized (Figure 2H, yellow insets). Since cofilin and myosin II compete for similar sites on actin filaments (Wiggan *et al.*, 2012), stimulation of CIE by cofilin depletion could be due to changes in myosin II activity. Indeed, we found that pRLC was increased in cofilin-silenced cell lysates (Supplemental Figure S1B), and treatment with blebbistatin blocked the enhancement of MHCI internalization induced by cofilin siRNA (Figure 2J) without effecting the level of pCFL (Supplemental Figure S1C). Thus, cofilin depletion affects CIE indirectly by altering myosin II activity, and CIE likely occurs independent of ROCK-mediated inactivation of cofilin's actin severing activity. The notion that myosin II contractility mediates CIE is surprising, as the role of actomyosin in endocytosis in vertebrate cells has been controversial (Liu *et al.*, 2009; Chandrasekar *et al.*, 2014). Whether other actin regulatory proteins downstream of ROCK proteins, like ERM proteins or adducins, might also play a role, remains to be determined.

Myosin IIA promotes internalization of MHCI and myosin IIB mediates internalization of CD59

To further understand how myosin II contractility regulates CIE, we asked whether specific myosin II isoforms mediate

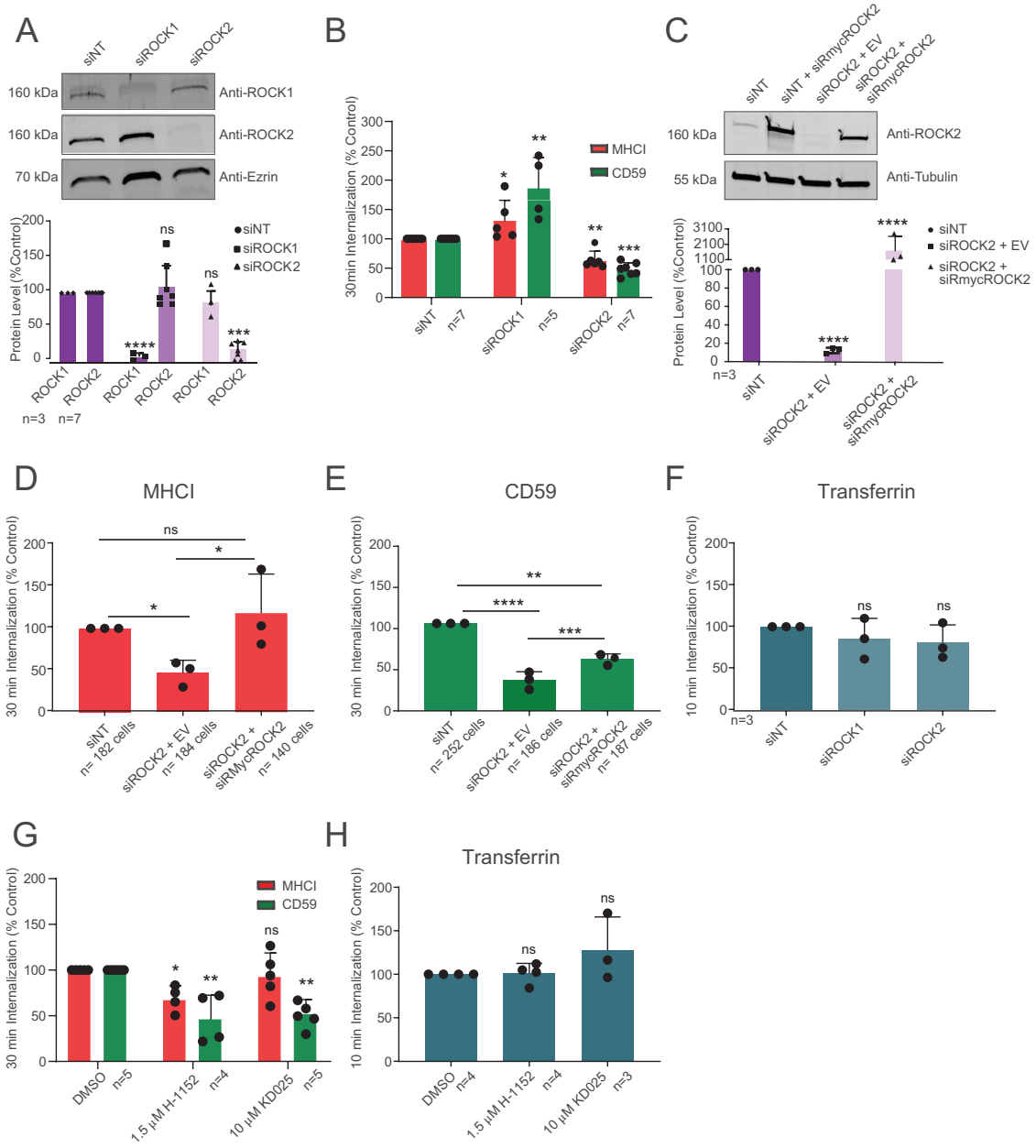

FIGURE 1: ROCK2, but not ROCK1, is required for internalization of CIE cargo proteins in HeLa cells. (A, C) Western blot and quantification of proteins isolated from siRNA-transfected HeLa lysates (siNT, control) with (C) or without (A) overexpression of either empty vector (EV) or siRNA-resistant myc-ROCK2 (siRmycROCK2). (B, D, E, G) Thirty-minute antibody internalization of MHCI (red) or CD59 (green) on HeLa cells with (D, E) or without (B) overexpression of either EV or siRmycROCK2, or after 30 min inhibitor pretreatment as indicated (G). (F, H) Ten-minute internalization of transferrin in siRNA-transfected HeLa cells (F) or after 30 min inhibitor pretreatment (H). *N* = total replicates (A, C) of six fields and approximately 25 cells per field (B, F–H) or number of cells (D, E) from at least three independent experiments; data expressed as mean ± SD (error bars). ns: $P > 0.05$; *$P \leq 0.05$; **$P \leq 0.01$; ***$P \leq 0.001$; ****$P \leq 0.0001$.

internalization of distinct CIE cargo. HeLa cells express myosin IIA and IIB, and both were effectively silenced with siRNA (Figure 3A). Surprisingly, we found that each CIE cargo protein required a unique myosin II isoform for their internalization. Silencing myosin IIA inhibited MHCI internalization (Figure 3B, left) leaving CD59 internalization unaffected (Figure 3B, right), while knockdown of myosin IIB strongly reduced CD59 internalization and only moderately affected MHCI internalization. Silencing myosin IIA modestly decreased transferrin internalization, while knockdown of myosin IIB had no effect (Figure 3C).

These results show that myosin II isoforms contribute to specific cargo internalization, with myosin IIA promoting MHCI endocytosis and myosin IIB mediating CD59 uptake. The notion that different CIE cargoes are internalized by molecularly distinct mechanisms has recently been brought to light by findings that galectin-glycan networks have differential effects on specific cargo internalization (Mathew and Donaldson, 2018), and different endophilin isoforms promote internalization of distinct CIE cargos (Renard *et al.*, 2020). Our results here, that two different CIE cargoes are regulated by a specific ROCK protein and distinct myosin II isoforms, support the

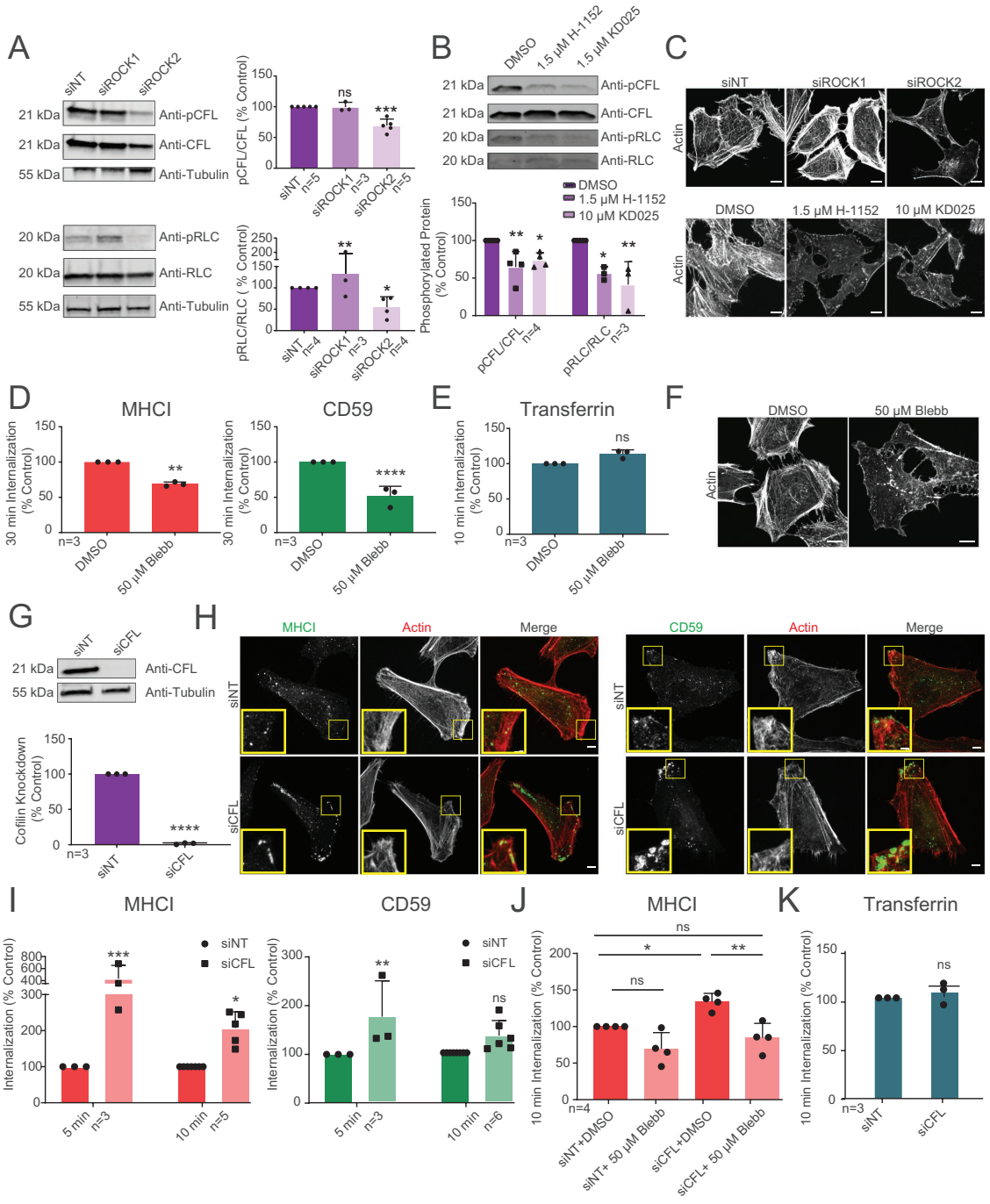

FIGURE 2: ROCK2 promotes CIE through regulation of myosin II contractility. (A, B, G) Western blot and quantification of phosphorylated (pCFL) or total cofilin (CFL), phosphorylated (pRLC) or total myosin light chain (RLC), or tubulin (A, G) from siRNA-transfected HeLa lysates, or after 30 min pretreatment with inhibitor or DMSO control (B). (D) Thirty-minute antibody internalization of MHCI or CD59 on HeLa cells following pretreatment with indicated inhibitor. (C, F, H) Maximum projections of confocal z-series of fluorescent phalloidin (C, F, H, red) or immunofluorescent staining of HeLa cells after 10 min antibody internalization for either MHCI or CD59 (H, green) after transfection of indicated siRNA (C,H), or after pretreatment with inhibitor or DMSO (C, F). Scale bars = 5 μm. Yellow boxes in H enlarged in insets, scale bar = 1 μm. (I, J) Five- (I) and 10-min (I, J) antibody internalization of MHCI or CD59 after siRNA transfection of HeLa cells, with (J) or without (I, J) pretreatment with inhibitor or DMSO (J). (E, K) Ten-minute internalization of transferrin following 30 min inhibitor pretreatment (E), or CFL siRNA transfection of HeLa cells (K). *N* = total replicates (A, B, G), of six fields and approximately 25 cells per field (D, I–K) from at least three independent experiments; data expressed as mean ± SD (error bars). ns: $P > 0.05$; *$P \leq 0.05$; **$P \leq 0.01$; ***$P \leq 0.001$; ****$P \leq 0.0001$.

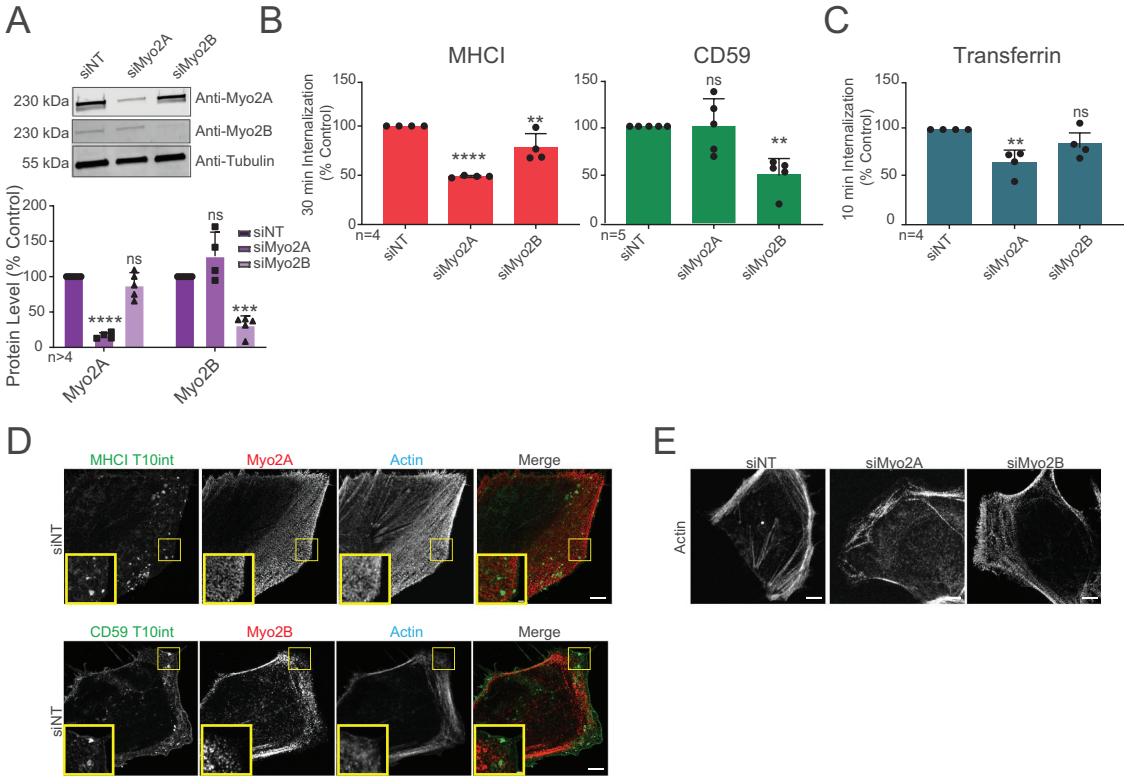

FIGURE 3: Myosin IIA promotes internalization of MHCI and myosin IIB mediates internalization of CD59. (A) Western blot and quantification of myosin IIA (Myo2A), myosin IIB (Myo2B), or tubulin from siRNA-transfected HeLa cells. (B) Thirty-minute antibody internalization of MHCI or CD59 or (C) 10-min internalization of transferrin on siRNA-transfected HeLa cells. (D, E) Maximum projections of confocal z-series in siRNA-transfected HeLa cells of fluorescent phalloidin and (E) immunofluorescent staining of Myo2A or Myo2B (red) after 10 min antibody internalization of either MHCI or CD59 (green). Scale bar = 5 μm. Yellow boxes in (D) enlarged in insets, bar, 1 μm. *N* = total replicates (A), of six fields and approximately 25 cells per field (B, C) from at least three independent experiments; data expressed as mean ± SD (error bars). ns: $P > 0.05$; *$P \leq 0.05$; **$P \leq 0.01$; ***$P \leq 0.001$; ****$P \leq 0.0001$.

idea that cargo-specific pathways of CIE are the rule rather than the exception.

Myosin IIA mediates internalization of MHCI from the basolateral domain and myosin IIB promotes CD59 uptake from the apical membrane of polarized intestinal epithelial cells

We next hypothesized that myosin II isoforms could regulate specific CIE cargo internalization in distinct cellular domains. Immunofluorescence of HeLa cells showed that myosin IIA and IIB exhibited largely similar localizations to peripheral arcs and stress fibers, with little direct overlap with internalized CD59 or MHCI (Figure 3D). siRNA silencing of either myosin IIA or IIB reduced arcs and stress fibers (Figure 3E); however, there was no obvious change in the localization of any residually internalized CIE cargo (Supplemental Figure S1D). Thus, in HeLa cells, it is unclear whether myosin II isoforms mediate regulation of specific CIE cargo internalization via spatial segregation.

We thus sought to examine the mechanism of myosin II isoform-dependent CIE cargo specificity in a system where both endocytosis and myosin II isoforms exhibit distinct spatial regulation. It is well-established in Caco2 intestinal epithelial cells that specific CME cargos localize and enter cells via distinct apical and basolateral domains (Cresawn *et al.*, 2007; Farr *et al.*, 2009), and for CIE, GPI-anchored proteins are known to reside on the apical domain (Paladino *et al.*, 2006). In addition, myosin II isoforms exhibit distinct functions and localizations in other polarized epithelial cell systems (Heuzé *et al.*, 2019). We first examined localizations of myosin IIA and IIB and the steady-state distribution of CIE cargoes in polarized Caco2 cells via 3D reconstruction of z-series of confocal optical sections (Figure 4, A and B). This showed both myosin II isoforms localized to the basal cortex, with myosin IIA additionally strongly enriched in the apical brush border where myosin IIB was minimal, and myosin IIB robustly localized to apical cell–cell junctions, where myosin IIA was excluded (Figure 4A; Supplemental Figure S2A). Analysis of CIE cargo showed that MHCI was strongly enriched at the lateral cell–cell contacts where CD59 was excluded, and CD59 was localized exclusively to the apical domain where MHCI was minimal (Figure 4B; Supplemental Figure S2B). We then determined whether CIE cargo proteins were internalized from a specific plasma membrane domain by apical or basal loading of cargo antibodies on confluent monolayers grown on filters in transwell chambers (Figure 4C). This showed that MHCI was exclusively internalized from basolateral-facing media, while CD59 was internalized only from apical-facing media (Figure 4C; Supplemental Figure S2C). Thus, myosin II isoforms and specific CIE cargo localization and internalization are at least partially spatially segregated in Caco2 intestinal epithelial cells.

The myosin II dependence of domain-specific cargo internalization was then tested by pharmacological inhibition or isoform-specific siRNA. Blebbistatin treatment reduced CIE of MHCI and CD59 from their respective basal and apical domains (Figure 4D). Myosin

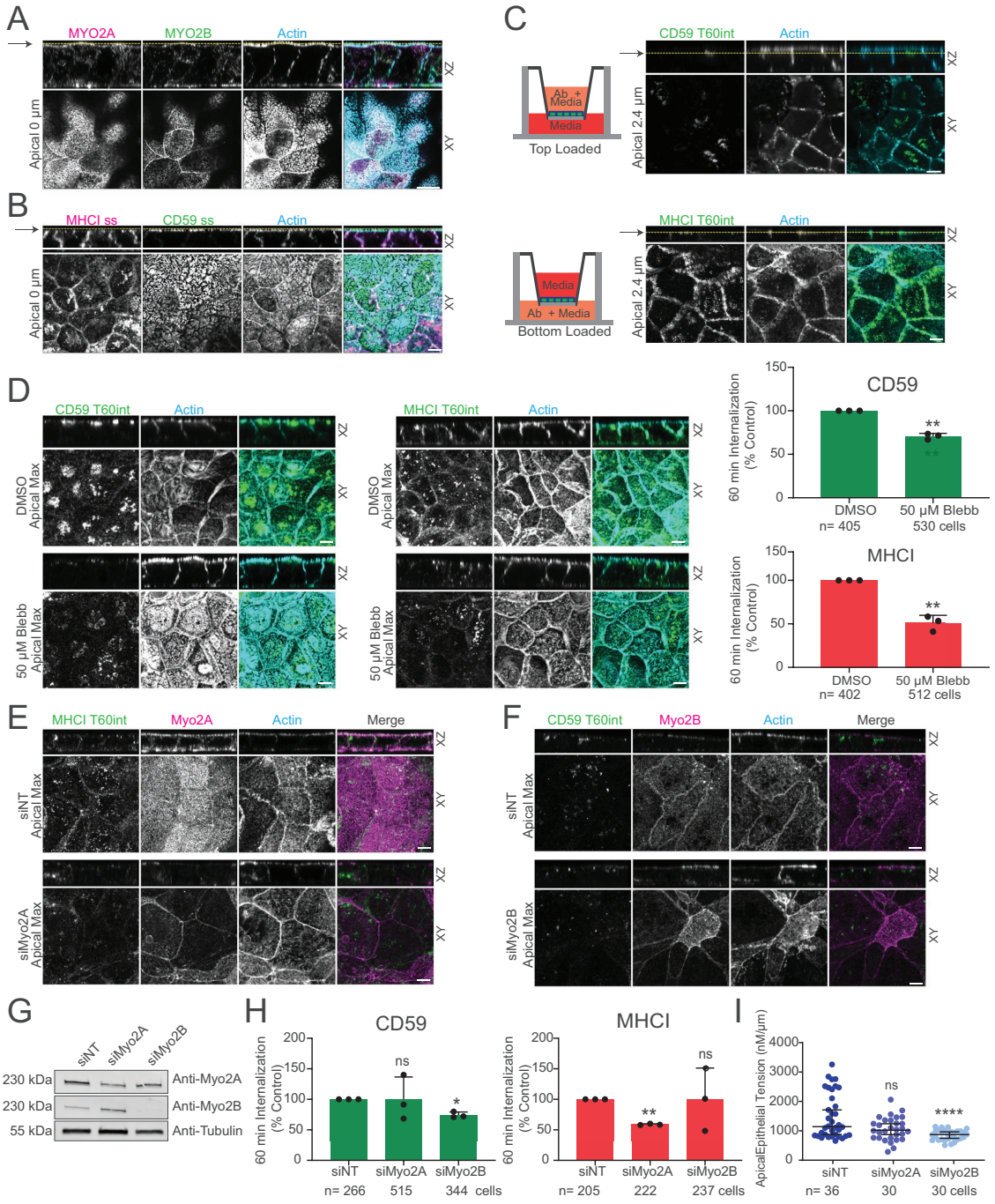

FIGURE 4: Myosin IIA mediates internalization of MHCI from the basolateral domain and myosin IIB promotes CD59 uptake from the apical membrane of polarized intestinal epithelial cells. (A–F) X-Z projections of confocal Z-series (above, XZ) and either a single X-Y confocal image (A–C below, Apical, XY) with the position of the Z-plane indicated by a yellow line and arrow and the distance from dorsal surface labeled or a maximum projection of the apical-most 1 µm (D–F, below, Apical Max, XY) of fluorescent phalloidin (Actin, blue) and immunostaining (as noted) in confluent monolayers of polarized Caco2 cells. Bars, 5 µm. (A) Immunostaining of myosin IIA (Myo2A, magenta) and myosin IIB (Myo2B, green) or (B) CD59 (green) and MHCI (magenta). (C–F) Sixty-minute internalization (T60int) and immunolocalization of antibodies to CD59 that were loaded apically (C, top; D, left; F) or to MHCI that were loaded basally (green, C [bottom]; D, center; E) on polarized Caco2 monolayers. (D) Cells were preincubated with either vehicle DMSO or inhibitor prior to antibody internalization. Quantification (right) of internalized MHCI and CD59. (E, F, H) Cells were transfected with indicated siRNA prior to internalization. (G) Western blot of proteins from siRNA-transfected Caco2 lysates isolated after 96 h transfection. (H) Quantification of internalized MHCI (red, right) and CD59 (green, left). (I) Cells were transfected with indicated siRNA prior to acoustic noncontact frequency-modulation AFM for determination of apical epithelial tension (nN/µm). *N* = number of cells from at least three independent experiments; data expressed as mean ± SD (error bars), except in I which is expressed at the median with 95% CI. ns: $P > 0.05$; *$P \leq 0.05$; **$P \leq 0.01$; ***$P \leq 0.001$; ****$P \leq 0.0001$.

IIA or IIB silencing substantially diminished protein levels in confluent polarized monolayers by 92 h posttransfection (Figure 4G; Supplemental Figure S2D), with minimal perturbation of epithelial morphology (Supplemental Figure S2, F and G), steady-state localization of cargo (Supplemental Figure S3A), or apico-basal polarity (Supplemental Figure S3B). However, inhibition of myosin IIA did result in a slight decrease in epithelial height (Supplemental Figure S3C). Analysis of CIE showed that knockdown of myosin IIA exclusively inhibited basal uptake of MHCI, while silencing myosin IIB only inhibited apically loaded anti-CD59 internalization (Figure 4, E–H; Supplemental Figure S2E).

Thus, in polarized intestinal epithelial cells, myosin IIA localizes at the basal cortex and apical brush border and mediates basolateral internalization of MHCI, while myosin IIB localizes to the basal cortex and apical cell–cell junctions and promotes CD59 uptake from the apical membrane. Although myosin IIA is most prominently localized at the brush border, it does not contribute to CIE of the apically internalized cargo, but myosin IIB at the apical junctions is critical. Instead, the fraction of myosin IIA at the basal cortex appears to be regulating basolateral CIE of MHCI. The fact that myosin II isoforms are not colocalized with their cargo both in HeLa and Caco2 cells rules out direct interactions and suggests the possibility that myosin II contractility in the cortical cytoskeleton could act "at a distance" to regulate plasma membrane tension to modulate the efficiency of CIE.

Myosin IIB regulates apical epithelial tension in polarized epithelial cells

We next sought to test the role of myosin II isoforms in regulating cortical tension. Although measurement of basolateral tension in cultured cells is not technically possible, acoustic noncontact frequency-modulation atomic force microscopy (FM-AFM; Gavara and Chadwick, 2010) allows measurement of apical epithelial tension in confluent epithelial monolayers (Cartagena-Rivera *et al.*, 2017). This analysis showed that depletion of myosin IIB strongly decreased apical epithelial tension while depletion of myosin IIA had a nonsignificant effect (Figure 4I). This suggests that myosin IIB at apical cell–cell junctions regulates dorsal cell-surface tension, and although myosin IIA is strongly localized to the dorsal cell surface, it does not contribute to apical tension. Our results support the contention that myosin II-mediated regulation of cortical tension, through interaction between the actin cytoskeleton and the plasma membrane, may be critical for efficient CIE. Decreased membrane tension has been shown to increase endocytic events in cases where actin polymerization (macropinocytosis; Loh *et al.*, 2019) or coat proteins (CME; Saleem *et al.*, 2015) are recruited to endocytic sites. As CIE has no clear requirement for either, it is not unreasonable to assume that lateral tension generated from myosin II contractility planar to the forming endocytic pit plays a large role in efficient CIE pit formation. When membrane tension is decreased, perhaps there is insufficient tension surrounding the pit to anchor the invaginating plasma membrane, and thus an endocytic pit cannot be efficiently formed. Further, the observation that endocytosis of CIE cargoes is stimulated in the case of excess NMII activation (in cofilin-silenced cells) would also suggest that balanced tension generated from NMII contractility is required for normal CIE. In support of this, the influence of NMII contractility on the endocytosis of CME cargoes has been observed by others (Chandrasekar *et al.*, 2014). Although we cannot rule out other possible roles for myosin II in cortical cytoskeleton organization, which may be required for nano-clustering of plasma membrane proteins (Goswami *et al.*, 2008), or vesicle fission through the recruitment of membrane bending proteins (Galic *et al.*, 2012), these possibilities remain to be tested in the future.

Here we show that ROCK2- and not ROCK1-mediated myosin II contractility promotes CIE, and that specific CIE cargoes demonstrate a distinct myosin II isoform requirement (Supplemental Figure S4). The idea that different CIE cargo proteins have unique mechanistic requirements supports the fact that identification of generalized requirements for CIE has remained elusive and suggests that viewing internalization of individual CIE cargos as unique endocytic pathways is a more appropriate angle by which to understand CIE.

MATERIALS AND METHODS

Cell culture

HeLa cells (ATCC, CCL-2) were cultured in EMEM (Lonza) supplemented with 10% fetal bovine albumin (FBS; Atlanta Biologicals), 1 mM sodium pyruvate (Life Technologies), 2 mM L-glutamine (Life Technologies), and 1% penicillin-streptomycin (considered complete EMEM).

Caco2 BBE cells were cultured in DMEM (Life Technologies) supplemented with 20% FBS (Atlanta Biologicals), 2 mM L-glutamine (Life Technologies), and 1% penicillin-streptomycin (considered complete DMEM). To establish polarized Caco2 cells, 12-well polystyrene transwell plates (Corning) were first incubated with complete DMEM in the upper and lower chamber at 37°C for at least 2 h to equilibrate. Adherent cells were lifted using TrypLE-express (Thermo Fisher) at 37°C for 10 min. Cells were then resuspended in 5 ml of complete DMEM and pelleted at 1000 × *g* for 5 min. Media were removed and cells were resuspended in 1 ml of complete DMEM, counted, and plated at 2.5×10^5 cells per transwell filter. Cells were then grown for 21 d (unless otherwise indicated) with 1× phosphate-buffered saline (PBS) washes and media changes every 3 d. All cells were maintained at 37°C in a humidified chamber with 5% CO_2.

Antibodies

Rabbit polyclonals used were to Ezrin (3145S, Cell Signaling Technology), pRLC (serine 19) (3671s, Cell Signaling Technology), myosin IIA (for immunofluorescence and Western blot, M8064, Sigma-Aldrich), and myosin IIB (for immunofluorescence PRB-455B, Covance). Rabbit monoclonal antibodies used were to cofilin (D3F9, Cell Signaling Technology) and ROCK1 (EP786Y, Abcam). Mouse monoclonals used were to CD59 (H19, BioLegend), CD59 (1F5, Sigma-Aldrich), MHCI (W6/32, BioLegend), ROCK2 (24A, Sigma-Aldrich), tubulin (T5168, Millipore Sigma), pCFL (serine 3) (E-5, Santa Cruz), RLC (K36, Millipore Sigma), myosin IIB (for Western blot, 3H2, Abcam), and ZO-1 (33-9100, Bethyl Laboratories). Alexa 488–conjugated transferrin and all secondary antibodies and phalloidin conjugated to Alexa Fluor 594, 488, or 647 were purchased from Molecular Probes. Alexa Fluor–conjugated 680 and 800 were purchased from Sigma-Aldrich.

DNA constructs and primers

The following constructs were used for overexpression experiments: pEGFP-N3 (Clontech, catalogue no. 6080-1) and murine myc-ROCK2. Mutagenesis PCR was performed using the site-directed II XL kit (Agilent) to create the siRNA-resistant myc-Rock2 with the following primers: 5′-catcgctagttagtgttctgtttgtttcttcaagagatgcaattgtagtat-3′ and 5′atactacaattgcatctcttgaagaaacaaacagaacactaactagcgatg-3′. All plasmids were sequenced to ensure accuracy.

siRNA transfections

HeLa cells were transfected with Dharmacon siRNA duplexes using Lipofectamine RNAimax (Thermo Fisher Scientific) following the manufacturer's instructions. Briefly, cells were lifted, pelleted, and resuspended in antibiotic-free complete EMEM; 1.5×10^5 cells were added to the siRNA transfection mixture and plated in 6-well dishes. Final concentration for all siRNA transfections was 40 nM. Cells were split 48 h posttransfection and plated onto coverslips at 1.5×10^5 cells per well of a 6-well plate and analyzed 24 h later for a total of 72 h siRNA knockdown, unless otherwise indicated.

Caco2 cells were transfected with Dharmacon siRNA duplexes using Lipofectamine RNAimax (Thermo Fisher Scientific) following the manufacturer's instruction. Briefly, cells were lifted, pelleted, and resuspended in antibiotic-free complete DMEM; 4.2×10^5 cells were added to siRNA transfection mixture and plated on transwell filters and allowed to polarize for 96 h (Clayburgh *et al.*, 2004). The final concentration of siRNA used was 100 nM. Media were changed daily until experimental manipulation.

A nontargeting siRNA sequence was used for siRNA controls (Dharmacon, ON-TARGETplus nontargeting pool). ROCK1 siRNA (Dharmacon, ON-TARGET plus human ROCK1 siRNA-smartpool), ROCK2 siRNA (Dharmacon, ON-TARGET plus human ROCK2 siRNA-smartpool), and cofilin siRNA (Dharmacon, ON-TARGET plus human CFL1 siRNA-smartpool) were used to silence expression of specific proteins of interest. After initial screening, all ROCK2 silencing was performed with a single ROCK2 sequence (Dharmacon, ON-TARGET plus human ROCK2 oligo 8 siRNA). Custom oligo sequences were used for silencing myosin IIA: sense: 5′-GGCCAAAGAGAACGAGAAGUU-3′ and antisense: 5′-CUUCUCGUUCUCUUUGGCCUU-3′ and for silencing myosin IIB: sense: 5′-AAGGAUCGCUACUAUUCAGGAUU-3′ and antisense: 5′UCCUGAAUAGUAGCGAUCCUUUU 3′ (Dharmacon).

Transfections

DNA transfections were performed on cells plated 1 d prior on coverslips at 0.5×10^5 cells per well in 6-well dishes using the Fugene HD (Promega) transfection reagent according to the manufacturer's instructions. Briefly, media in a 6-well dish were replaced with 2 ml of fresh complete EMEM. A transfection mixture consisting of 100 µl of Optimum, 6 µl of Fugene HD, and 1 µg DNA was incubated at 15 min at room temperature (RT) and then added to each well of a 6-well plate. After 4 h, wells were washed briefly with 1× PBS and fresh complete EMEM was added. Experiments were performed 24 h posttransfection.

For rescue experiments, cells were transfected with siRNA and plated on coverslips at 1.5×10^5. After 6 h, media were removed and fresh complete media were added; 24 h later, DNA transfection of the siRNA-resistant myc-ROCK2 construct or the Empty Vector control was performed and an endocytosis assay was performed 24 h post-DNA transfection for a total of 48 h siRNA silencing and 24 h DNA overexpression.

Endocytosis assays

Endocytosis was measured in HeLa cells using antibody (or transferrin) internalization assays as follows: after the indicated incubations, transfections, or pretreatments, cells on coverslips were placed face down on parafilm onto 50 µl of medium containing primary antibody at concentrations of 5 µg/ml for CD59 (H19; BioLegend) and 10 µg/ml for MHCI (W6/32; BioLegend) or 10 µg/ml Alexa Fluor 488–linked transferrin (Molecular Probes). Coverslips underwent continuous antibody or transferrin uptake by incubating for the indicated time at 37°C while background control coverslips were incubated on ice. After antibody uptake, one set of coverslips that was incubated at 37°C was fixed in 2% formaldehyde (representing total antibody bound both internally and to the surface of the cell, T_{tot}), and another set of coverslips that was held at 37°C (representing antibody internalized, T_{int}) as well as the set that was kept on ice (null control, T_0) were acid-washed for 60 s using a solution of 0.5% acetic acid, 0.5 m NaCl, pH 3.0, after which these sets of coverslips were fixed and immunofluorescence staining was performed. Briefly, cells were blocked for 20 min in 10% FBS in 1× PBS, then incubated with Alexa Fluor anti-mouse 488 and cell mask deep red (Thermo Fisher) for 1 h at RT. Cells were then washed 3× in 1× PBS and mounted with Fluoromount (Thermo Fisher) onto glass slide and allowed to cure for 30 min before imaging. Prior to transferrin internalization, cells were serum-starved for 30 min at 37°C to clear unlabeled transferrin present in complete media.

Endocytosis assays were performed in Caco-2 cells as follows: Caco-2 cells were allowed to form a polarized monolayer on transwell filters in a 12-well dish for 21 d, with the exception of siRNA-treated cells that were quickly polarized for 96 h (as described above). After the indicated incubations, transfections, or pretreatments, cells were incubated with 5 µg/ml for CD59 (1F5; Thermo Fisher) and 10 µg/ml for MHCI (W6/32; BioLegend) or 10 µg/ml Alexa Fluor 488–linked transferrin (Molecular Probes) in the transwell supports. For top-loaded assays: primary antibody diluted in 200 µl of DMEM to the final concentration stated above was added to the apical-facing surface of Caco-2 cells, while 400 µl of complete DMEM alone were added to the basolateral-facing surface to allow internalization of antibody to occur only from the apical domain. For bottom-loaded assays: 200 µl of complete DMEM alone were added to the apical-facing surface, while primary antibody diluted in 400 µl of complete DMEM to the final concentration stated above was added to the basolateral-facing surface to allow internalization to occur only from the basolateral domain. Once it was determined that CD59 was internalized apically (top-loaded) and MHCI was internalized basolaterally (bottom-loaded), all subsequent assays were performed from that domain for that cargo. All internalization was performed at 37°C for 60 min, after which cells were quickly rinsed with cold PBS and acid-washed for 60 s using a solution of 0.5% acetic acid, 0.5 m NaCl, pH 3.0, to visualize internalized antibody, with the exception of Figure 4B which was not acid stripped to allow visualization of endogenous, steady-state localization.

Inhibitor treatments

HeLa cells were plated onto coverslips 24 h prior to drug treatment at 1.5×10^5 cells per well of a 6-well dish. Inhibitors, or DMSO vehicle control, were resuspended in serum-free media to the following final working concentrations: 50 µM blebbistatin (Sigma), 10 µM KD025 (Cayman Chemical), and 1.5 µM H1152 (Cayman Chemical). Cells were pretreated with the indicated inhibitor for 30 min prior to experimental assay at 37°C, followed by endocytosis assays in the presence of the inhibitor for the indicated times. Lysates for Western blotting were isolated from cells that were treated with the indicated inhibitor for 60 min. Caco2 cells were allowed to polarize on transwell filters for 21 d prior to inhibitor treatments and were pretreated with the indicated inhibitor for 60 min prior to experimental assay at 37°C.

Immunostaining

HeLa cells were plated on coverslips at least 24 h prior to manipulation. Cells were fixed in 2% paraformaldehyde in PBS for 20 min at RT, washed 3× with PBS, and then blocked for 20 min in 10% FBS in PBS. Primary and secondary antibody incubations were performed

for 1 h at RT in the presence of 0.2% saponin (Sigma-Aldrich), separated by three washes in PBS. Coverslips that were used for quantification of endocytosis were incubated with 2 μg/ml HCS cell mask deep red stain (Molecular Probes) with the indicated secondary antibody. In conditions where two different mouse isotype primary antibodies were used, IgG-specific anti-mouse secondaries were utilized. Coverslips were mounted in Fluoromount (Thermo Fisher) mounting media and allowed to cure for at least 30 min before imaging.

Caco2 cells grown on transwell filters were fixed in ice-cold 100% ethanol at 4°C for 20 min, followed by two washes in PBS. Filters were then excised from the wells with a scalpel and blocked in 4% FBS in PBS for 1 h at RT. Primary antibody incubation was performed in 4% FBS in PBS overnight at 4°C in a humid chamber. Secondary antibody incubation was performed 4% FBS in PBS at RT for 1 h. Transwell filters were mounted face up under a coverslip with Prolong Gold (Thermo Fisher) mounting media.

Western blot

Protein samples for Western blot analysis were obtained from cells washed briefly in cold 1× PBS and directly lysed in 2× sample buffer diluted from 4× sample buffer stocks (200 mm Tris-HCl, pH 6.8, 4% β-mercaptoethanol, 8% SDS, 0.4% bromophenol blue, and 40% glycerol) and boiled for 2 min. Samples were run on precast 4–20% SDS–PAGE gradient gels (Bio-Rad) and semidry transferred onto PVDF membranes using the Trans-Blot Turbo System (Bio-Rad). Membranes were then blocked in 5% milk in 1× Tris-buffer saline (TBS) for 1 h at RT. Antibody incubations were diluted in 3% BSA in TBS + 0.1% Tween-20 (TBS-T) and all washes were in TBS-T. Primary antibody incubations were performed overnight at 4°C and Alexa Fluor 680 and 800 secondary antibody incubations were performed for 1 h at RT. Primary and secondary antibody incubations were separated by three washes for 5 min each. Membranes were visualized using the LI-COR Odyssey Imager (LI-COR).

Confocal microscopy

For quantification of endocytosis in HeLa cells, coverslips were imaged at RT using a confocal microscope (LSM 780 FCS, Carl Zeiss) with a 40× Plan-Apo oil immersion objective and 488- and 633-nm laser excitation. For each coverslip, six stage positions were imaged with 2 × 2 tiling with the confocal pinhole kept completely open, with an average of 25–50 cells per position. All images were acquired with the same settings and quantified using MetaMorph software (Molecular Devices).

For quantification of endocytosis in Caco2 cells, coverslips were imaged at RT using a confocal microscope (LSM 780 FCS, Carl Zeiss) with a 63× Plan-Apo oil immersion objective and 488- and 594-nm laser excitation. Confocal z-stacks were acquired with a 1-μm step size. All images were acquired with the same settings and quantified using ImageJ (National Institutes of Health [NIH]).

All other imaging was superresolution confocal microscopy, which was performed on an LSM 880 (Carl Zeiss) equipped with an Airyscan detector, with a 63× Plan-Apo oil immersion objective and 488-, 594-, and 633-nm laser excitation. Confocal z-stacks were acquired with a 0.2-μm step-size. All images were postprocessed using ZEN black (Carl Zeiss)

Image analysis, processing, and data presentation

MetaMorph software (Molecular Devices) was used to quantify endocytic internalization in HeLa cells. Confocal images were separated into separate TIF images and an antibody channel threshold was set for each condition using its T_0 coverslip images. T_0 is the background control coverslip that has been subjected to an antibody internalization assay but is held on ice for the duration of the experiment, then washed, acid-stripped, and fixed. Immunofluorescence procedure is then performed as normal (see *Endocytosis assays* in *Materials and Methods* above for more details). When imaged, the fluorescence intensity measured from this sample is subtracted as background (thresholded) from all other samples from the experiment for that day. The T_{int} and T_{tot} conditions were then thresholded, and the integrated signal intensity was measured for the antibody channel where T_{int} is a coverslip that has been subjected to an antibody internalization for the time stated at 37°C, then washed, acid stripped, and fixed. Immunofluorescence is then performed as normal. This coverslip represents the internal amount of antibody that was internalized into the cell, and T_{tot} is a coverslip that has been subjected to antibody internalization for the time stated at 37°C, then washed and fixed without an acid wash step. This coverslip represents the total amount of surface and internalized antibody in the cell.

The cell mask channel was auto-thresholded, and the threshold area was measured and the integrated signal intensity for the antibody was then normalized to the threshold area for each image. The percentage internalized was then calculated with the equation: % internal = $100 \times (T_{tot/area})/(T_{int/area})$. Approximately 100 cells were measured for each experiment (at least six fields, with an average of 25 cells per field), with experiments performed at least in triplicate. For graphing purposes, the percentages were normalized to the untreated control as indicated.

ImageJ software was used to quantify endocytic internalization in Caco2 cells. First, SUM projections of two apical confocal slices were created. Individual cells were then circled and the integrated intensity of the internalized antibody (in arbitrary units) was measured on a per cell basis. All data are presented as a percentage of the nontreated control condition. In cases of siRNA treatment, the cells were costained for the protein that was targeted for knockdown to determine efficient siRNA silencing on a per-cell basis, and only cells with sufficient protein knockdown were selected for quantification.

Noncontact acoustic frequency-modulation atomic force microscopy

Caco2 cells transfected with control, myosin IIA, or myosin IIB siRNA were plated at high density and cultured for 96 h on transwell filters to allow for monolayer polarization. The transwell filters with monolayers were gently cut from the transwell chambers and glued with superglue (Loctite) onto a glass-bottom dish (Willco Wells). Such Caco2 polarized monolayers were then subjected to noncontact FM-AFM (Gavara and Chadwick, 2010; Cartagena-Rivera *et al.*, 2017, 2019). FM-AFM experiments were performed utilizing a Bruker Bioscope Catalyst Atomic Force Microscope system (Bruker) mounted on an inverted Axiovert 200 M optical microscope (Carl Zeiss) equipped with a confocal laser scanning microscope 510 Meta (Carl Zeiss) using a 40× objective lens (0.95 NA, Plan-Apochromat; Carl Zeiss). During experiments, monolayers were maintained at 37°C using a heating sample stage (Bruker). A modified AFM microcantilever with an attached 25-μm polystyrene bead (Novascan) was used for all FM-AFM measurements. Using the thermal tune fluctuations method built in the AFM system, the calibrated spring constants for the cantilevers were 0.55–0.7 N/m. Next, the monolayer was placed on the AFM sample stage and tapping mode was selected. Then, the cantilever tune curve mode was engaged and the cantilever driving frequency was chosen to be the largest frequency peak near the cantilever natural resonance frequency

(predetermined by the thermal tune method). After gently engaging the monolayer apical surface, the cantilever tune was launched, and the cantilever was positioned at 6 µm away from the monolayer. Then, a frequency sweep was recorded, and the cantilever phase lag was corrected to be $\pi/2$. Next, the acoustically vibrating bead was moved from the 6-µm to 1-µm gap distance by 500-nm intervals. A frequency sweep was recorded for each interval. Supracellular apical epithelial tension calculations were performed using a custom-made MATLAB program (MathWorks). The apical epithelial tension model based on lubrication theory for linearized Stokes flow used herein can be accessed for detailed description (Cartagena-Rivera *et al.*, 2017).

Statistical analysis

At least three independent biological replicates were carried out for each experiment, and data were expressed as mean ± SD. All statistical analysis was performed using Prism 8 (GraphPad software). In experiments with multiple comparisons, statistical significance was determined using a one-way ANOVA with a Dunnett's posttest to compare means of different samples with the control. Mann–Whitney tests were performed in cases where data wer not assumed to be normally distributed. In experiments with only two conditions, an unpaired Student's *t* test was used to determine statistical significance. Statistical significance was considered for *p* values that were > 0.05. For all figures, ns: $P > 0.05$; *$P \leq 0.05$; **$P \leq 0.01$; ***$P \leq 0.001$; ****$P \leq 0.0001$.

ACKNOWLEDGMENTS

The authors thank Xufeng Wu and the National Heart, Lung, and Blood Institute (NHLBI) Light Microscopy Core Facility for microscopy expertise; Schwanna Thacker for administrative support; and Koji Shimomura for assistance with analysis. J.W., D.D., J.G.D., and C.M.W. were supported by the Division of Intramural Research of NHLBI and A.C.-R. was supported by NIBIB and the NIH Distinguished Scholars Program.

REFERENCES

Amano M, Ito M, Kimura K, Fukata Y, Chihara K, Nakano T, Matsuura Y, Kaibuchi K (1996). Phosphorylation and activation of myosin by Rho-associated kinase (Rho- kinase). J Biol Chem 271, 20246–20249.

Amano M, Nakayama M, Kaibuchi K (2010). Rho-kinase/ROCK: A key regulator of the cytoskeleton and cell polarity. Cytoskeleton 67, 545–554.

Bhadriraju K, Yang M, Alom Ruiz S, Pirone D, Tan J, Chen CS (2007). Activation of ROCK by RhoA is regulated by cell adhesion, shape, and cytoskeletal tension. Exp Cell Res 313, 3616–3623.

Boucrot E, Ferreira APA, Almeida-Souza L, Debard S, Vallis Y, Howard G, Bertot L, Sauvonnet N, McMahon HT (2015). Endophilin marks and controls a clathrin-independent endocytic pathway. Nature 517, 460–465.

Boulant S, Kural C, Zeeh JC, Ubelmann F, Kirchhausen T (2011). Actin dynamics counteract membrane tension during clathrin-mediated endocytosis. Nat Cell Biol 13, 1124–1132.

Bucher D, Frey F, Sochack KA, Kummer S, Bergeest JP, Godinez WJ, Kräusslich HG, Rohr K, Taraska JW, Schwarz US, *et al.* (2018). Clathrin-Adaptor ratio and membrane tension regulate the flat-To-curved transition of the clathrin coat during endocytosis. Nat Commun 9, 1–13.

Cartagena-Rivera AX, Le Gal S, Richards K, Verpy E, Chadwick RS (2019). Cochlear outer hair cell horizontal top connectors mediate mature stereocilia bundle mechanics. Sci Adv 5, eaat9934.

Cartagena-Rivera AX, Van Itallie CM, Anderson JM, Chadwick RS (2017). Apical surface supracellular mechanical properties in polarized epithelium using noninvasive acoustic force spectroscopy. Nat Commun 8, 1–12.

Chadda R, Howes MT, Plowman SJ, Hancock JF, Parton RG, Mayor S (2007). Cholesterol-sensitive Cdc42 activation regulates actin polymerization for endocytosis via the GEEC pathway. Traffic 8, 702–717.

Chandrasekar I, Goeckeler ZM, Turney SG, Wang P, Wysolmerski RB, Adelstein RS, Bridgman PC (2014). Nonmuscle myosin II is a critical regulator of clathrin-mediated endocytosis. Traffic 15, 418–432.

Clayburgh DR, Rosen S, Witkowski ED, Wang F, Blair S, Dudek S, Garcia JGN, Alverdy JC, Turner JR (2004). A differentiation-dependent splice variant of myosin light chain kinase, MLCK1, regulates epithelial tight junction permeability. J Biol Chem 279, 55506–55513.

Cresawn KO, Potter BA, Oztan A, Guerriero CJ, Ihrke G, Goldenring JR, Apodaca G, Weisz OA (2007). Differential involvement of endocytic compartments in the biosynthetic traffic of apical proteins. EMBO J 26, 3737–3748.

Damke H, Baba T, Warnock DE, Schmid SL (1994). Induction of mutant dynamin specifically blocks endocytic coated vesicle formation. J Cell Biol 127, 915–934.

Day CA, Baetz NW, Copeland CA, Kraft LJ, Han B, Tiwari A, Drake KR, Luca HD, Chinnapen D, Davidson MW, *et al.* (2015). Microtubule motors power plasma membrane tubulation in clathrin-independent endocytosis. Traffic 16, 572–590.

Farr GA, Hull M, Mellman I, Caplan MJ (2009). Membrane proteins follow multiple pathways to the basolateral cell surface in polarized epithelial cells. J Cell Biol 186, 269–282.

Galic M, Jeong S, Tsai FC, Joubert LM, Wu YI, Hahn KM, Cui Y, Meyer T (2012). External push and internal pull forces recruit curvature-sensing N-BAR domain proteins to the plasma membrane. Nat Cell Biol 14, 874–881.

Gavara N, Chadwick RS (2010). Noncontact microrheology at acoustic frequencies using frequency-modulated atomic force microscopy. Nat Methods 7, 650–654.

Gold ES, Underhill DM, Morrissette NS, Guo J, McNiven MA, Aderem A (1999). Dynamin 2 is required for phagocytosis in macrophages. J Exp Med 190, 1849–1856.

Goswami D, Gowrishankar K, Bilgrami S, Ghosh S, Raghupathy R, Chadda R, Vishwakarma R, Rao M, Mayor S (2008). Nanoclusters of GPI-anchored proteins are formed by cortical actin-driven activity. Cell 135, 1085–1097.

Greathouse KM, Boros BD, Deslauriers JF, Henderson BW, Curtis KA, Gentry EG, Herskowitz JH (2018). Distinct and complementary functions of rho kinase isoforms ROCK1 and ROCK2 in prefrontal cortex structural plasticity. Brain Struct Funct 223, 4227–4241.

Hak LCW, Khan S, Meglio IDi, Law AL, Häsler SLA, Quintaneiro LM, Ferreira APA, Krause M, McMahon HT, Boucrot E (2018). Fbp17 and cip4 recruit ship2 and lamellipodin to prime the plasma membrane for fast endophilin-mediated endocytosis. Nat Cell Biol 20, 1023.

Henley JR, Krueger EWA, Oswald BJ, McNiven MA (1998). Dynamin-mediated internalization of caveolae. J Cell Biol 141, 85–99.

Heuzé ML, Sankara Narayana GHN, D'Alessandro J, Cellerin V, Dang T, Williams DS, Van Hest JCM, Marcq P, Mège RM, Ladoux B (2019). Myosin II isoforms play distinct roles in adherens junction biogenesis. Elife 8.

Johnson DL, Wayt J, Wilson JM, Donaldson JG (2017). Arf6 and Rab22 mediate T cell conjugate formation by regulating clathrin-independent endosomal membrane trafficking. J Cell Sci 130, 2405–2415.

Julian L, Olson MF (2014). Rho-associated coiled-coil containing kinases (ROCK), structure, regulation, and functions. Small GTPases 5, e29846.

Kimura K, Ito M, Amano M, Chihara K, Fukata Y, Nakafuku M, Yamamori B, Feng J, Nakano T, Okawa K, *et al.* (1996). Regulation of myosin phosphatase by Rho and Rho-associated kinase (Rho- kinase). Science (80-) 273, 245–248.

Kumari S, Mayor S (2008). ARF1 is directly involved in dynamin-independent endocytosis. Nat Cell Biol 10, 30–41.

Levayer R, Pelissier-Monier A, Lecuit T (2011). Spatial regulation of Dia and Myosin-II by RhoGEF2 controls initiation of E-cadherin endocytosis during epithelial morphogenesis. Nat Cell Biol 13, 529–540.

Liu AP, Loerke D, Schmid SL, Danuser G (2009). Global and local regulation of clathrin-coated pit dynamics detected on patterned substrates. Biophys J 97, 1038–1047.

Loh J, Chuang MC, Lin SS, Joseph J, Su YA, Hsieh TL, Chang YC, Liu AP, Liu YW (2019). An acute decrease in plasma membrane tension induces macropinocytosis via PLD2 activation. J Cell Sci 132, 1242.

Maekawa M, Ishizaki T, Boku S, Watanabe N, Fujita A, Iwamatsu A, Obinata T, Ohashi K, Mizuno K, Narumiya S (1999). Signaling from Rho to the actin cytoskeleton through protein kinases ROCK and LIM-kinase. Science (80-) 285, 895–898.

Maldonado-Báez L, Williamson C, Donaldson JG (2013). Clathrin-independent endocytosis: A cargo-centric view. Exp Cell Res 319, 2759–2769.

Mathew MP, Donaldson JG (2018). Distinct cargo-specific response landscapes underpin the complex and nuanced role of galectin–glycan interactions in clathrin-independent endocytosis. J Biol Chem 293, 7222–7237.

Naslavsky N, Weigert R, Donaldson JG (2003). Convergence of non-clathrin- and clathrin-derived endosomes involves Arf6 inactivation and changes in phosphoinositides. Mol Biol Cell 14, 417–431.
Paladino S, Pocard T, Catino MA, Zurzolo C (2006). GPI-anchored proteins are directly targeted to the apical surface in fully polarized MDCK cells. J Cell Biol 172, 1023–1034.
Radhakrishna H, Donaldson JG (1997). ADP-ribosylation factor 6 regulates a novel plasma membrane recycling pathway. J Cell Biol 139, 49–61.
Rauskolb C, Sun S, Sun G, Pan Y, Irvine KD (2014). Cytoskeletal tension inhibits Hippo signaling through an Ajuba-Warts complex. Cell 158, 143–156.
Renard HF, Simunovic M, Lemière J, Boucrot E, Garcia-Castillo MD, Arumugam S, Chambon V, Lamaze C, Wunder C, Kenworthy AK, *et al*. (2015). Endophilin-A2 functions in membrane scission in clathrin-independent endocytosis. Nature 517, 493–496.
Renard HF, Tyckaert F, Lo Giudice C, Hirsch T, Valades-Cruz CA, Lemaigre C, Shafaq-Zadah M, Wunder C, Wattiez R, Johannes L, *et al*. (2020). Endophilin-A3 and Galectin-8 control the clathrin-independent endocytosis of CD166. Nat Commun 11.
Renard HF, Johannes L, Morsomme P (2018). Increasing Diversity of Biological Membrane Fission Mechanisms. Trends Cell Biol 28, 274–286.
Riento K, Ridley AJ (2003). Rocks: Multifunctional kinases in cell behaviour. Nat Rev Mol Cell Biol 4, 446–456.
Sabharanjak S, Sharma P, Parton RG, Mayor S (2002). GPI-anchored proteins are delivered to recycling endosomes via a distinct cdc42-regulated clathrin-independent pinocytic pathway. Dev Cell 2, 411–423.
Saleem M, Morlot S, Hohendahl A, Manzi J, Lenz M, Roux A (2015). A balance between membrane elasticity and polymerization energy sets the shape of spherical clathrin coats. Nat Commun 6, 1–10.
Sandvig K, Kavaliauskiene S, Skotland T (2018). Clathrin-independent endocytosis: an increasing degree of complexity. Histochem Cell Biol 150, 107–118.
Sathe M, Muthukrishnan G, Rae J, Disanza A, Thattai M, Scita G, Parton RG, Mayor S (2018). Small GTPases and BAR domain proteins regulate branched actin polymerisation for clathrin and dynamin-independent endocytosis. Nat Commun 9, 1–16.
Shi J, Wu X, Surma M, Vemula S, Zhang L, Yang Y, Kapur R, Wei L (2013). Distinct roles for ROCK1 and ROCK2 in the regulation of cell detachment. Cell Death Dis 4.
Soriano-Castell D, Chavero A, Rentero C, Bosch M, Vidal-Quadras M, Pol A, Enrich C, Tebar F (2017a). ROCK1 is a novel Rac1 effector to regulate tubular endocytic membrane formation during clathrin-independent endocytosis. Sci Rep 7, 1–17.
Soriano-Castell D, Chavero A, Rentero C, Bosch M, Vidal-Quadras M, Pol A, Enrich C, Tebar F (2017b). ROCK1 is a novel Rac1 effector to regulate tubular endocytic membrane formation during clathrin-independent endocytosis. Sci Rep 7, 1038.
Thottacherry JJ, Sathe M, Prabhakara C, Mayor S (2019). Spoiled for choice: diverse endocytic pathways function at the cell surface. Annu Rev Cell Dev Biol 35, 55–84.
Traub LM, Bonifacino JS (2013). Cargo recognition in clathrin-mediated endocytosis. Cold Spring Harb Perspect Biol 5, 1101.
Wiggan O, Shaw AE, DeLuca JG, Bamburg JR (2012). ADF/Cofilin regulates actomyosin assembly through competitive inhibition of Myosin II binding to F-actin. Dev Cell 22, 530–543.